Large Influence of Cholesterol on Solute Partitioning into Lipid Membranes

Christian L. Wennberg,[†] David van der Spoel, and Jochen S. Hub*,[‡]

Department of Cell and Molecular Biology, Uppsala University, Husargatan 3, Box 596, SE-75124 Uppsala, Sweden

S *Supporting Information*

ABSTRACT: Cholesterol plays an important role in maintaining the correct fluidity and rigidity of the plasma membrane of all animal cells, and hence, it is present in concentrations ranging from 20 to 50 mol %. Whereas the effect of cholesterol on such mechanical properties has been studied exhaustively over the last decades, the structural basis for cholesterol effects on membrane permeability is still unclear. Here we apply systematic molecular dynamics simulations to study the partitioning of solutes between water and membranes. We derive potentials of mean force for six different solutes permeating across 20 different lipid membranes containing one out of four types of phospholipids plus a cholesterol content varying from 0 to 50 mol %. Surprisingly, cholesterol decreases solute partitioning into the lipid tail region of the membranes much more strongly than expected from experiments on macroscopic membranes, suggesting that a laterally inhomogeneous cholesterol concentration and permeability may be required to explain experimental findings. The simulations indicate that the cost of breaking van der Waals interactions between the lipid tails of cholesterol-containing membranes account for the reduced partitioning rather than the surface area per phospholipid, which has been frequently suggested as a determinant for solute partitioning. The simulations further show that the partitioning is more sensitive to cholesterol (i) for larger solutes, (ii) in membranes with saturated as compared to membranes with unsaturated lipid tails, and (iii) in membranes with smaller lipid head groups.
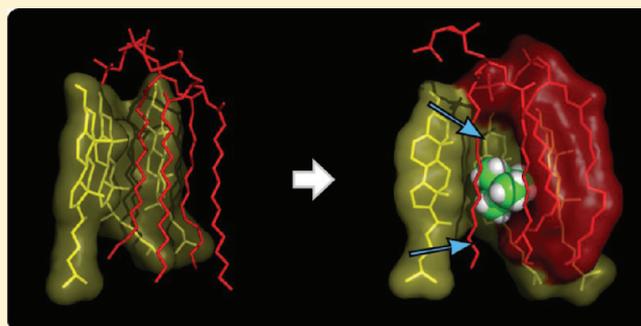
INTRODUCTION

Understanding and predicting the permeability of lipid membranes, based on the membrane composition and the properties of the permeating solute, is one of the central goals in membrane biology. Membrane permeation is involved in numerous physiological functions, but it also plays an important pharmacological role because most drugs are required to enter the cells via diffusion across lipid membranes. A widely used model to describe the permeability P of a membrane with respect to a specific permeating solute is the solubility-diffusion model, assuming that the inverse of P can be expressed as an integral over the membrane,

$$\frac{1}{P} = \int_{-d/2}^{d/2} \frac{\mathrm{d}z}{K(z)\,D(z)} \tag{1}$$

Here, d denotes the thickness of the membrane, z is the coordinate along the membrane normal, and $K(z)$ and $D(z)$ are the position-dependent partition coefficient and diffusion constant of the solute, respectively.

How the partitioning and the diffusion are controlled by determinants such as the lipid type or cholesterol content, as well as by solute hydrophobicity, size, and shape, has been subject to extensive experimental investigation.[1−6] Complementary, molecular dynamics (MD) simulations have evolved to become a mature technique to investigate the quantities underlying the permeability coefficients.[7−12] In line with ESR measurements using spin-labeled lipids,[13] these simulation studies demonstrated that the concentration (or partitioning) of solutes as well as the diffusion constants vary along the membrane normal.[8,10−12] When comparing different solutes, the diffusion constants inside lipid membranes differ only by factors of 2−3 in a given membrane,[9,12] whereas partition coefficients may vary by orders of magnitude,[3] constituting the latter as the main determinant for permeability. Therefore, we here focus on solute partitioning, noting, however, that the diffusion constant may influence the permeability to some extent as well.

Here, we study the influence of cholesterol on the permeability of biological membranes. Cholesterol is abundant in the plasma membrane of animal cells at molar concentrations ranging from 20% to 50%.[14] Cholesterol acts as a precursor for hormones and vitamin D, and it functions in signaling across membranes. In addition to such metabolic functions, it plays an important role in maintaining the proper fluidity and rigidity of the membrane.[15] The role of cholesterol on the membrane structure has therefore been studied extensively over the years using experimental[16−18] and computational techniques.[19−25]

Table 1. Composition of Simulation Systems (number of phospholipid/cholesterol/water molecules)

phospholipid	cholesterol-free	20% cholesterol	30% cholesterol	40% cholesterol	50% cholesterol
POPE	128/0/4777	120/30/4455	100/42/4621	90/60/3799	80/80/4697
POPC	128/0/5788	100/24/3274	100/42/4374	80/54/4529	80/80/4496
DMPC	100/0/4216	100/24/4221	100/42/5316	80/54/5323	70/70/5330
DPPC	100/0/4117	100/24/4111	100/42/5224	80/54/5230	70/70/5257

From these and other studies, the ordering and condensing effects of cholesterol on the membrane are well-documented.[15]

In contrast, the effect of cholesterol on the primary biological function of lipid membranes, that is, the formation of a barrier against solute permeation, is much less understood. In early experiments a moderate reduction of membrane permeability was measured for water, ions, or glucose upon the addition of cholesterol, typically by a factor of 2−4.[26−28] Complementary, the partitioning of solutes such as benzene, molecular oxygen, anesthetics, or druglike compounds into the membrane has been found to be moderately reduced by cholesterol by factors of approximately 2−6.[13,29−33] More recently, spectroscopic and fluorescence experiments demonstrated that the effect of cholesterol on the partitioning of water or molecular oxygen into lipid membranes is more pronounced in membranes of saturated lipids as compared to membranes of unsaturated lipids.[13,33] That finding is explained by the fact that kinks in unsaturated lipid tails prevent a favorable packing with the planar cholesterol molecules, leaving a larger amount of free volume in the membrane. In some studies a more pronounced decrease in permeability through cholesterol was observed by a factor of ∼25 in certain membranes.[34,35] Computationally, potentials of mean force (PMFs) for a number of small solutes permeating across dimyristoylphosphatidylcholine (DMPC)/cholesterol mixed membranes were estimated using Widom's particle insertion method,[36] and the permeation of hypericin across cholesterol-containing membranes has been addressed.[37]

A quantitative understanding of cholesterol effects on membrane permeability is still missing. One uncertainty, which has so far not been addressed in the context of membrane permeation, is the lateral distribution of cholesterol over the membrane. In membranes containing both saturated and unsaturated phospholipids, cholesterol is not equally distributed but instead accumulates in so-called lipid rafts.[38,39] In addition, even in membranes containing merely one type of phospholipid, cholesterol may not be homogeneously distributed but can instead induce the coexistence of liquid disordered and liquid ordered phases with low and high local cholesterol content, respectively,[40,41] although the coexistence of different liquid phases is still controversial.[42] Consequently, solutes may predominantly permeate the membrane at positions with low local cholesterol concentration and thus high local permeability. Other determinants of the permeability of cholesterol-containing membranes are likewise poorly understood. Besides the saturation of the lipid chains, such determinants include the type of lipid headgroup or the size of the solute.

Therefore, we here present an extensive molecular dynamics study on the partitioning of a set of solutes in cholesterol-containing membranes. We have built and equilibrated 20 membrane systems containing cholesterol plus one type of phospholipid, either palmitoyloleylphosphatidylethanolamine (POPE), palmitoyloleylphosphatidylcholine (POPC), DMPC, or dipalmitoylphosphatidylcholine (DPPC). The cholesterol concentration was varied between 0 and 50 mol % in the

simulations, in the range of physiological conditions. Subsequently, we have employed the technique of umbrella sampling to compute potentials of mean force (PMFs) $G(z)$ for the permeation of ethanol, ammonia, nitric oxide, propane, benzene, and neopentane across all 20 membranes, covering a wide range of solute size and solute hydrophobicity. Because the PMFs were defined to zero in the bulk water regimes, they are directly related to the partition coefficient via $K(z) = \exp[-G(z)/k_BT]$, where k_B and T denote the Boltzmann constant and the temperature, respectively. The PMFs thus allow us to detect, besides the effects of cholesterol, the influence of the type of lipid tails and head groups, as well as the impact of solute size on the partitioning. Remarkably, the simulations suggest that cholesterol reduces the local permeability much more strongly than expected from permeation experiments on macroscopic membranes.

■ METHODS

Simulation Setup, Parameters, and Equilibration. Equilibrated patches of pure POPE or pure POPC were taken from a previous study.[43] All other membranes were built by placing lipid molecules at evenly distributed positions on a square grid for each monolayer, yielding lipid bilayers containing between 100 and 160 lipids. (With the term "lipid" we here always refer to both phospholipids and cholesterol.) The bilayers were then solvated with at least 3274 TIP4P[44] water molecules. The composition of all simulation systems is summarized in Table 1. The systems were energy minimized using a conjugate gradient algorithm. Thereafter, the systems containing purely phospholipids were equilibrated for at least 40 ns. Systems containing cholesterol plus POPE, POPC, or DMPC were equilibrated for 200 ns. Systems containing cholesterol plus DPPC equilibrated slowly and were therefore equilibrated for 700 ns.

All simulations were carried out using the Gromacs simulation software.[45,46] Parameters for POPE, POPC, and DMPC were based on the work of Berger et al.,[47] with the modifications for the oleoyl double bond and for the ethanolamine group being those introduced by Tieleman and Berendsen.[48] The DPPC model was taken from Ulmschneider and Ulmschneider, which is based on more recent experimental data.[49] Cholesterol parameters were taken from Höltje et al.,[50] and the OPLS all-atom force field[51,52] was applied for ammonia, ethanol, propane, benzene, and neopentane. Lennard-Jones parameters for nitric oxide were taken from Cohen et al.,[53] and the partial charges were computed by density function theory using the B3LYP functional[54−56] with the aug-cc-pVTZ basis set[57,58] in the Gaussian 2003 suite.[59] The charges were fitted to reproduce the electrostatic potential produced by the quantum chemistry calculation,[60,61] yielding ±0.0215e for the oxygen and the nitrogen atom, respectively, where e denotes the proton charge. During equilibration, the temperature was controlled at 300 K (323 K for DPPC) through velocity rescaling[62] (τ = 2 ps), and the pressure was kept at 1 bar using the weak coupling scheme[63] (τ = 1 ps). The SETTLE[64] algorithm was applied to constrain bond lengths and angles of water molecules, and LINCS[65] was used to constrain all other bond lengths, allowing a time step of 2 fs. Electrostatic interactions were calculated at every step using the particle-mesh Ewald method,[66,67] and dispersive interactions were described by a Lennard-Jones potential with a cutoff at 1 nm.

The potential energy between the lipid tail atoms, V_{tails}, was derived from the average sum of Lennard-Jones and short-range Coulomb potentials between all pairs of atoms in the lipid tail region. For

cholesterol, all atoms except for the hydroxyl group were included, and for phospholipids, all tail atoms up to the three glycerol carbon atoms were included. The potential energy was averaged over the last 10 and 100 ns of the equilibrium simulations for cholesterol-free and cholesterol-containing simulations, respectively. Statistical errors for V_{tails} were derived by binning analysis.[68]

Umbrella Sampling Simulations. Starting structures for the umbrella simulations were taken from randomly chosen snapshots of the last 5 ns and the last 20 ns of the cholesterol-free and cholesterol-containing equilibrium simulations, respectively. The membrane normal z was chosen as reaction coordinate for solute permeation, where $z = 0$ nm is defined by the center of mass (COM) of the lipid and cholesterol molecules. Here, the COM was computed using a weighted sum over the membrane atoms within a cylinder of radius 12 Å, centered at the respective solute and aligned along the z-axis. Here, a weight of 1 was assigned to all atoms within a distance of 8 Å to the cylinder axis, and the weights were switched to 0 between 8 and 12 Å. That procedure avoids artifacts in the PMF due to undulation of the membrane. The reaction coordinate was divided into 264−392 equidistant sections, with each section representing the center of an umbrella window. Adjacent umbrella windows were separated by 0.25 Å, and the umbrella windows spanned the complete space between one bulk water region across the membrane and into the other bulk water region.

Solutes were inserted at the umbrella centers. To save computational resources, four or five different umbrella windows were sampled within each simulation, keeping a distance of 15 Å along z for propane, nitric oxide, and ammonia and a distance of 20 Å for ethanol, benzene, and neopentane. In addition, to further reduce the statistical error, four solutes were sampled within each umbrella window simultaneously, where the four solutes were separated by approximately half the width of the simulation box in the x−y plane. Hence, 16−20 umbrella histograms could be collected from each umbrella simulation. Water molecules which overlapped with the solute were removed. Overlaps between the solute and lipid atoms were removed by gradually switching on Lennard-Jones interactions between the solute and the rest of the system within 1000 simulation steps, using soft-core Lennard-Jones potentials and a stochastic dynamics integration scheme. Subsequently, the energy of each structure was minimized. Two typical simulation systems, containing either purely phospholipids or phospholipids and cholesterol, are shown in Figure 1.

A harmonic umbrella potential acting on the center of mass of the solute was applied (force constant 1000 kJ mol^{-1} nm^{-2}). Each umbrella simulation was carried out for 1 ns. The temperature was set to 300 K through a stochastic dynamics integrator ($\tau = 0.1$ ps). The pressure was controlled at 1 bar by the semi-isotropic Parrinello−

Rahman[69] barostat, scaling the box in the x−y plane only, but keeping the box dimension in the z-direction fixed.

Construction of PMFs. After removing the first 200 ps for equilibration, the PMFs were computed using a periodic version of the weighted histogram analysis method (WHAM),[70] as implemented in the g_wham software.[71] Depending on the system, the PMFs were based on 1056 to 1568 histograms. Here, the integrated autocorrelation times (IACTs) of the umbrella windows were incorporated in the WHAM iteration procedure as described by Kumar et al.[70] IACTs were estimated as described in ref 71, and smoothed along z using a Gaussian filter with $\sigma = 0.2$ nm. The final PMFs were symmetrized around the membrane center ($z = 0$).

Statistical uncertainties of the PMFs were calculated using the Bayesian bootstrap of complete histograms.[71] This procedure yields reliable uncertainties because it does not depend on accurate autocorrelation time estimates. Instead, the procedure considers only complete histograms as independent data points.

Below we compare the PMFs to hexadecane/water partition coefficients, K_{hex}. K_{hex} of ammonia, ethanol, nitric oxide, and benzene were taken from the literature.[3,72−74] K_{hex} of propane was approximated by the cyclohexane/water partition coefficient taken from ref 75. Because the experimental K_{hex} of neopentane is (to our knowledge) not available, we computed the respective K_{hex} through the PMF for neopentane across a hexadecane/water slab, as explained in the supporting material of ref 76, yielding $\log_{10} K_{hex} = 3.8 \pm 0.3$.

Convergence of Cholesterol-Containing Simulations. We carefully checked the convergence of the equilibration simulations through the potential energy and box dimensions of the systems. In addition, we computed the PMF for the permeation of ammonia across the POPE/30% cholesterol and across POPC/30% cholesterol systems as a function of the equilibration time of the membrane patch (Figure S1, Supporting Information), suggesting that 200 ns equilibration is sufficient for systems containing POPE, POPC, DMPC plus cholesterol. In contrast, systems composed of DPPC and cholesterol carried out the slow transition to the liquid ordered phase on the time scale of several 100 ns. Consequently, an equilibration time of 700 ns was applied for these systems. The equilibrated systems are available for download on one of the author's (J.S.H.) Web site at http://cmb.bio.uni-goettingen.de.

Apart from the equilibration of the membrane patches, we validated explicitly that 1 ns of umbrella simulation, while discarding the first 200 ps for equilibration, is sufficient. Accordingly, a number of PMFs were computed with increasing equilibration time (typically between 50 and 800 ps). The calculated PMFs did not show a systematic trend with increasing equilibration time, suggesting that 200 ps are sufficient. In addition, the calculation of one PMF (ammonia across POPC/40% cholesterol) was carried out using 100-ns instead of 1-ns umbrella simulations. The PMFs based on equilibration times between 200 ps and 95 ns do again not show a systematic trend and agree within the statistical error with the result based on 1-ns simulations (Figure S2, Supporting Information).

Moreover, we recomputed (parts of) three PMFs using Widom's test particle insertion (TPI) method[77] (Methods, Supporting Information). In contrast to umbrella sampling, TPI calculations do not require that the membrane equilibrates with respect to an inserted solute, but solutes are instead inserted into random frames from equilibrium simulation of the pure membrane. The PMFs from TPI favorably agree with the umbrella sampling results (Figure S3, Supporting Information), suggesting again that the umbrella sampling simulations are not biased by insufficient equilibration.

Figure 1. Typical simulation systems of membranes of (A) pure POPC and (B) POPC plus 40 mol % cholesterol. POPC molecules are shown in gray, cholesterol in blue, and water in red/white. A number of benzene molecules, as present in umbrella sampling simulations, are shown in green/white sphere representation and 2-nm scales are indicated by magenta rods.

■ RESULTS

Permeation across Pure Phospholipid Membranes. Because the present study focuses on the effect of cholesterol on membrane permeability, we discuss only the general features of PMFs for pure phospholipid membranes. These PMFs mainly serve as a reference for the following sections on cholesterol-containing membranes.
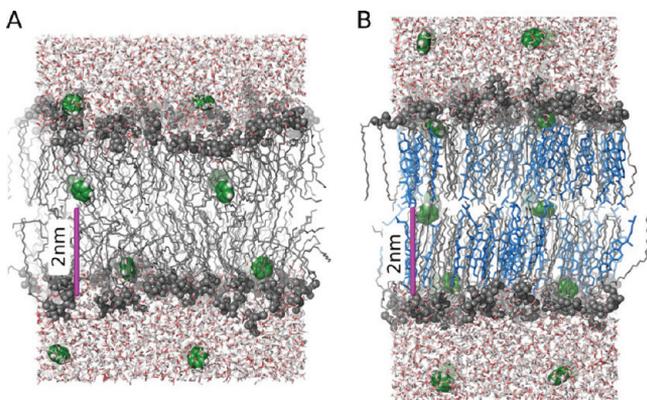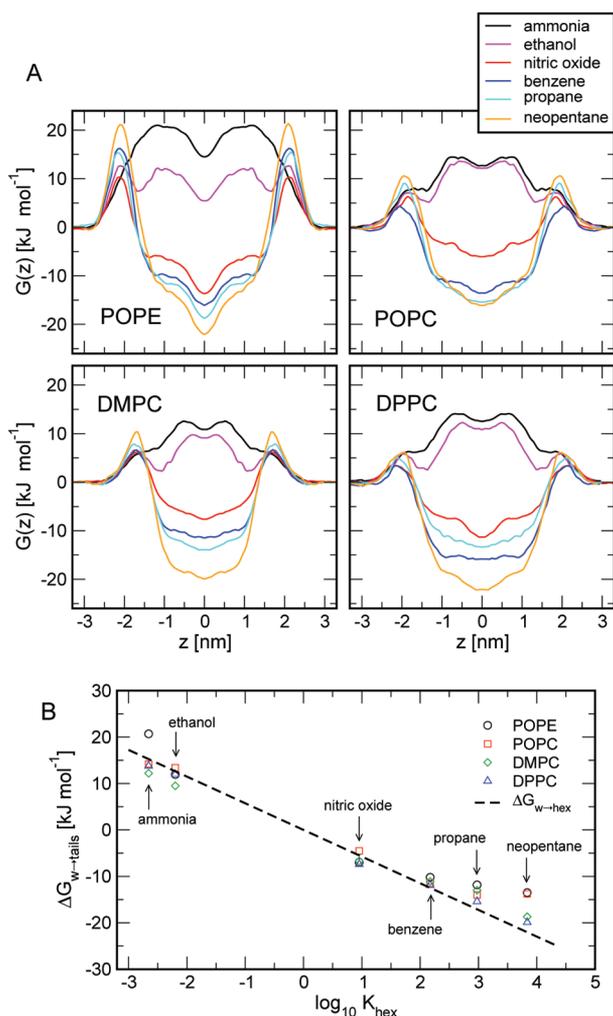
Figure 2. Partitioning in pure phospholipid membranes. (A) Potentials of mean force (PMFs) for the permeation of ammonia (black), ethanol (magenta), nitric oxide (red), benzene (blue), propane (cyan), and neopentane (orange) across membranes of pure POPE, POPC, DMPC, and DPPC, as indicated in the graphs. Data for POPE, POPC, and DMPC corresponds to a temperature of 300 K and DPPC data to 323 K. (B) Transfer free energy $\Delta G_{w\rightarrow tails}$ for moving a solute from bulk water into the lipid tail regions of the PMFs. $\Delta G_{w\rightarrow tails}$ is plotted versus the logarithm of the hexadecane/water partition coefficient log K_{hex} of the respective solute. Different symbols indicate $\Delta G_{w\rightarrow tails}$ in different membranes, as shown in the legend. The dashed line corresponds to the free energy $\Delta G_{w\rightarrow hex} = - k_B T \ln K_{hex}$ for moving the solute from water to hexadecane.

Figure 2A presents the PMFs for ammonia, ethanol, nitric oxide, propane, benzene, and neopentane permeating across membranes of pure POPE, POPC, DMPC, or DPPC. PMF in Figure 2A were symmetrized between the two leaflets in order to incorporate the symmetry of the membrane. Nonsymmetrized PMFs are shown in Figure S4 (Supporting Information). Whereas all PMFs for POPE, POPC, and DMPC correspond to a temperature of 300 K, all DPPC PMFs were derived at 323 K to avoid the transition to the gel phase. The color coding of the curves is explained in the figure legend. $z = 0$ represents the center of the bilayer. The lipid tails are located in the region $|z| \leq 1.5$ nm, and lipid head groups are located around $|z| \sim 2$ nm.

As previously pointed out,[7,8,10] PMFs are by no means flat across the membrane, but instead the structural inhomogeneity of the membrane is reflected in four main features of the PMFs.

The first feature is a nearly flat PMF in the two bulk water regimes at $|z| > 2.5-3$ nm. The second feature is a barrier for hydrophobic solutes at the lipid head groups (HGs) around $|z| \approx 2$ nm. That barrier is more pronounced in the POPE membrane than in any of the three phosphatidylcholine (PC) membranes, suggesting that strong salt bridges between the phosphatidylethanolamine (PE) HGs as well as hydrogen bonds between PE HGs and nearby water molecules are required to break upon the insertion of a solute. As expected, that barrier increases with the size and hydrophobicity of the solute. The larger the solute, the more HG–HG and HG–water interactions are lost upon permeation. The more hydrophobic the solute, the lower is its ability to replace these lost interactions by solute–HG interactions. In PC HGs, where the positive charge is shielded by three methyl groups, the polar interactions of the HGs are weaker, rationalizing the lower HG barriers in the PC membranes. The third feature is the region of the lipid tails around $|z| \sim 1$ nm, where the maxima of the PMFs for ammonia and ethanol are located (Figure 2A, black and magenta curves) and where the PMFs for the hydrophobic solutes are flat or saddle point shaped. Because, in addition to the maxima in the PMFs, the diffusion constant was shown to be low in the lipid tail region,[8,10] that region is expected to constitute the rate-limiting resistance against full permeation events of polar solutes. In the following sections we show that the addition of cholesterol increases the excess free energy for a solute in that region. The fourth and final feature is a local minimum at the center of the bilayer ($|z| \lesssim 0.3$ nm). That region is characterized by a reduced lipid tail density and increased free volume.[8] Hence, a solute located at this position does not break van der Waals contacts between lipid tails, rationalizing the more favorable free energy.

Figure 2B relates the PMFs to Overton's rule, stating that the permeability of a given membrane is proportional to the hexadecane/water (or oil/water) partition coefficient.[78] The graph plots the transfer free energies for moving a solute from bulk water to the tail regions of the four membranes near $|z| \approx 1$ nm, denoted $\Delta G_{w\rightarrow tails}$, versus hydrophobicity of the solute, as measured from the logarithm of the hexadecane/water partition coefficient log$_{10}$ K_{hex}. $\Delta G_{w\rightarrow tails}$ (circles, squares, diamonds, and triangles) is compared to the transfer free energy for moving a solute from water to hexadecane $\Delta G_{w\rightarrow hex}$ (dashed line). In line with Overton's rule, the overall trend of $\Delta G_{w\rightarrow tails}$ agrees favorably with $\Delta G_{w\rightarrow hex}$, yielding confidence in the applied simulation parameters and protocols. However, $\Delta G_{w\rightarrow tails}$ for a specific solute may differ by a few kilojoules/mole in different membranes. For instance, $\Delta G_{w\rightarrow tails}$ for ammonia equals 21 and 14.5 kJ/mol for POPE and POPC, respectively, suggesting that solute partitioning is not purely determined by the solute hydrophobicity but, in addition, is altered by the packing of the specific lipid. These findings agree to experimentally observed effects from chain ordering and lipid density on solute partitioning into lipid membranes.[5,32]

Now, that we have established the physicochemical characteristics of partitioning in pure phospholipid membranes and have compared these results to previous studies, we turn toward the effects of the addition of cholesterol.

PMFs of Cholesterol-Containing Membranes. Figure 3 presents the PMFs for solutes permeating across membranes with an increasing cholesterol content [Chol] between 0 and 50 mol %. Because the PMFs were symmetrized over the two membrane leaflets, we here show only the PMF for one leaflet, ranging from the center of the membrane at $z = 0$ nm to into
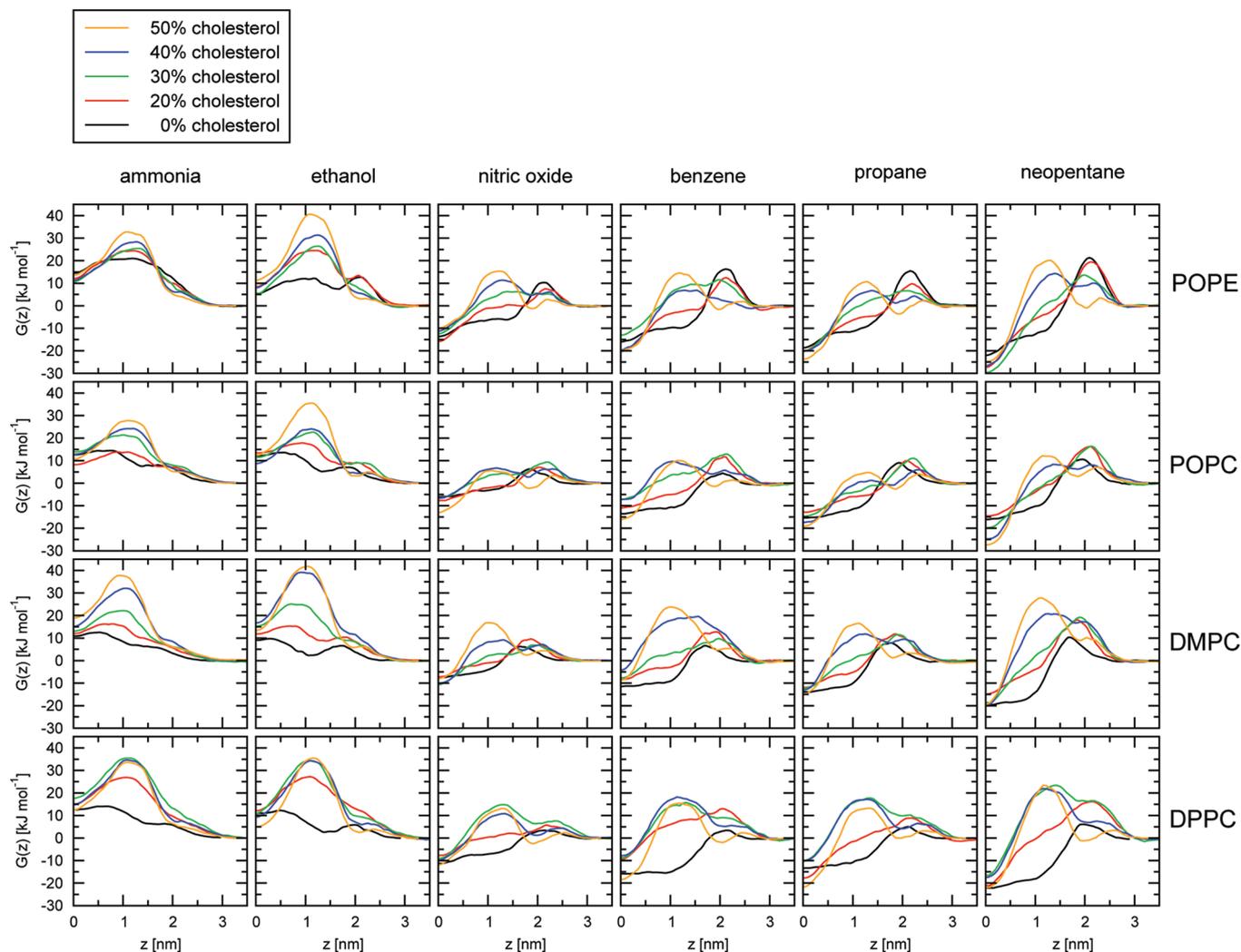
5354

dx.doi.org/10.1021/ja211929h | *J. Am. Chem. Soc.* 2012, 134, 5351–5361

Figure 3. Partitioning in cholesterol-containing membranes. Potentials of mean force for the permeation of (from left column to right column) ammonia, ethanol, nitric oxide, benzene, propane, and neopentane. The rows present PMFs of membranes containing different types of phospholipids. From top to bottom: POPE, POPC, DMPC, and DPPC, as indicated on the right-hand side. The color of the curves encode the cholesterol content (see legend): black, 0%; red, 20%; green, 30%; blue, 40%; orange, 50% cholesterol. The PMFs are shown only for one leaflet of the membrane, ranging from the center of the membrane at $z = 0$ nm to the bulk water at $z = 3.5$ nm.

the bulk water at $z \approx 3$ nm. Nonsymmetrized PMFs are shown in Figure S5 (Supporting Information). In Figure 3, each column represents a specific solute, while each row shows the PMFs for membranes containing one specific phospholipid (POPE, POPC, DMPC, or DPPC). The colors of the curves encode the cholesterol content of 0% (black), 20% (red), 30% (green), 40% (blue), and 50% (orange). Hence, the PMFs in Figure 2A are shown in Figure 3 as black curves to allow the visual comparison to the PMFs for cholesterol-containing membranes.

With increasing cholesterol concentration ([Chol]), all PMFs increase in the lipid tail region around $z \approx 1$ nm, where the bulky polycyclic groups of cholesterol are located (Figure 1B). Because the PMFs were defined to zero in the bulk water regimes, that increase corresponds to an increase in the transfer free energy $\Delta G_{w \rightarrow tails}$ for moving a solute from the bulk water into the lipid tail region or, in turn, to a decrease of the respective solute partition coefficient $K_{w \rightarrow tails} = \exp[-\Delta G_{w \rightarrow tails}/k_B T]$. Depending on the solute and the type of phospholipid, $\Delta G_{w \rightarrow tails}$ increases between 10 and 45 kJ/mol upon the addition of 50 mol % cholesterol, corresponding to a

strong decrease of the partition coefficient by 2−7 orders of magnitude. That decrease is much more pronounced than in experiments on macroscopic membranes (see Discussion).

In the very center of the membrane at $z \approx 0$, in contrast, the PMFs are nearly unaffected by [Chol] (Figure 3). That finding is in line with the simulation snapshots of cholesterol-containing membranes (Figure 1B). Cholesterol molecules do not extend into the membrane center and, therefore, do not enhance the packing at $z \approx 0$. Because the PMFs strongly increase at $|z| \approx 1$ nm with increasing [Chol], however (last paragraph), solutes solvated in the hydrophobic part of the membrane are consequently increasingly concentrated into the center of the membrane. That finding further suggests that the partitioning of solutes to an arbitrary position in the membrane is much less affected by [Chol] than the partitioning in the lipid tail region. Experiments that probe the spacially averaged solute partitioning in the membrane, but do *not* probe the partitioning in a z-dependent manner, may therefore not detect the strong cholesterol effect in the lipid tail region around $|z| \approx 1$ nm.

Apart from the change in the lipid tail region, the PMFs are affected in the headgroup regions by cholesterol. The most

drastic changes at the head groups are observed in the PMFs for the bulky and hydrophobic neopentane and benzene, and these changes are most pronounced in the POPE membranes. Remarkably, these substantial barriers at the head groups at $z \approx$ 2 nm are reduced by the addition of ~30% cholesterol, and they nearly vanish upon the addition of 50% cholesterol (Figure 3; see subplots benzene/POPE and neopentane/POPE). Because the $\Delta G_{w \rightarrow tails}$ simultaneously increases with [Chol], the lowest overall barrier is found at a moderate [Chol] of ~30%. Assuming that the headgroup barrier is rate-limiting for the permeation of benzene or neopentane across pure POPE, that finding suggests that the addition of ~30% cholesterol would increase the permeability of POPE membranes for bulky hydrophobic solutes.

The permeability of a membrane is mainly determined by the highest barrier or, equivalently, by the membrane region with the smallest partition coefficient, as directly follows from eq 1. In the following discussion, we therefore focus on the effect of cholesterol in the lipid tail region, where the strongest increase in free energy is observed upon the addition of cholesterol. Figure 4 presents $\Delta G_{w \rightarrow tails}$ versus the cholesterol concentration
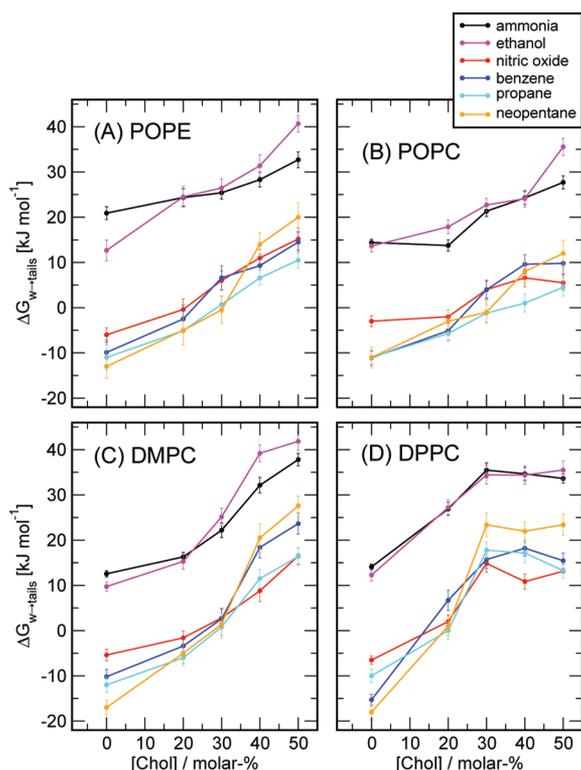

Figure 4. Transfer free energies $\Delta G_{w \rightarrow tails}$ for moving the solutes from bulk water into the lipid tail region of cholesterol-containing membranes of membranes of (A) POPE, (B) POPC, (C) DMPC, and (D) DPPC. The color of the curves indicates the type of solute (see legend).

[Chol], as taken from from the 120 PMFs in Figure 3. If the respective PMF displays a barrier in the lipid tail region (e.g., all ammonia and ethanol PMFs, as well as all PMFs at high [Chol]), the value in Figure 4 equals the barrier height. In contrast, if no such barrier is present in the lipid tail region (hydrophobic solutes at low [Chol]), the value in Figure 4 was taken from the flat or saddle-point-shaped part of the PMF near $z = 1$ nm. Such values should therefore be considered as

approximate only. In addition, as pointed out in the previous paragraph, $\Delta G_{w \rightarrow tails}$ do not in all cases reflect the highest and, thus, the rate-limiting barrier against solute permeation. Figure 4 demonstrates that the increase in $\Delta G_{w \rightarrow tails}$ not only depends on [Chol] but also on the size of the solute, the lipid tails, and the type of lipid headgroup.

(1) In all membranes, the increase in $\Delta G_{w \rightarrow tails}$ is more pronounced for larger neopentane and benzene molecules, as compared to the smaller ammonia or nitric oxide molecules. These findings are in line with the well-known condensing effect of cholesterol, leading to a smaller area per phospholipid and, hence, to a decrease in free volume inside the bilayer.[15,24] Figure 4 shows that the partitioning of larger solutes is more strongly affected by that reduction of the free volume.

(2) $\Delta G_{w \rightarrow tails}$ increases more strongly with [Chol] in membranes of saturated lipid tails as compared to membranes of unsaturated tails, as can be inferred by comparing $\Delta G_{w \rightarrow tails}$ in DMPC (Figure 4C) with the values in POPE or POPC (Figure 4A/B). That feature is in qualitative agreement with experiments that found a larger decrease in permeability or partitioning in saturated as compared to unsaturated lipids after the addition of cholesterol,[13,28,33] and it can be rationalized by the double bond in the oleoyl chains of POPE and POPC, which induces a kink in the hydrocarbon chain and thus precludes any tight packing with the planar and rigid cholesterol molecules.[25] Consequently, more disorder and free volume remains in the POPE/cholesterol and POPC/cholesterol membranes, leading a slower increase of $\Delta G_{w \rightarrow tails}$ with [Chol] as compared to the DMPC/cholesterol membranes.

(3) Besides the lipid tail, the lipid head groups affect the increase of $\Delta G_{w \rightarrow tails}$ with [Chol]. By comparing the curves for POPE and POPC (Figure 4A/B), we find that, for all solutes except for ammonia, the increase in $\Delta G_{w \rightarrow tails}$ is more pronounced in lipids with the small PE as compared to larger PC headgroup. Due to the large head groups of POPC, the area per lipid of 68 Å^2 is substantially larger than the area per lipid in POPE, which equals approximately 50 Å^2.[79−81] The lipid tail region of POPC is therefore more disordered (see also Figure 1A) and allows for more free volume compared to POPE. Our results demonstrate that a larger molar fraction of cholesterol is required in POPC to "fill" the free volume and, as a consequence, to reduce the solute partitioning. On the basis of these findings, we conclude that the permeability of membranes with small head groups is more sensitive to the addition of cholesterol than the permeability of membranes with larger head groups.

(4) For DPPC, $\Delta G_{w \rightarrow tails}$ is nearly constant for [Chol] ≥ 30% (Figure 4D). That behavior is different from that of all other membranes considered here, but it may be explained by the phase behavior of DPPC/cholesterol membranes. Experiments showed that DPPC membranes carry out transitions to more ordered phases (liquid ordered or gel phase) at lower cholesterol concentrations and/or lower temperature as compared to POPC and DMPC membranes.[41,82] At 300 K—the temperature employed for our simulations of POPE, POPC, and DMPC—pure DPPC adopts the gel phase in

the experiment[40] and in our simulations (data not shown). To keep the focus here on the physiologically relevant liquid phases, we decided to carry out all DPPC simulations at 323 K. However, at 323 K and only 20% cholesterol, visual inspection of the simulation showed that the DPPC membrane adopted a liquid-ordered phase, that is, at slightly lower cholesterol content than expected from experiments and thermodynamic modeling.[40] At 30% cholesterol, the DPPC tails were highly ordered, and the ordering did not increase further with higher [Chol], rationalizing why $\Delta G_{w \to tails}$ does not further increase with [Chol].[40]

Structural Determinants for PMFs. Having analyzed the increase in $\Delta G_{w \to tails}$ and, hence, the decrease in solute partitioning in the membrane with [Chol], we turn toward possible structural explanations for that phenomenon. De Young and Dill found that the partitioning of benzene into cholesterol-containing PC membranes decreases with cholesterol content between 0% and 40%, and that this decrease is correlated with the increase of the phospholipid surface density.[32] Complemented by a mean field lattice theory for solubility,[83] these and other authors[35] therefore emphasized lipid surface area as an important determinant for the permeability of cholesterol-containing membranes. More recently, Mathai et al. found that the water permeability of pure phospholipid membranes correlates with the area per lipid.[6] However, these authors attributed the correlation to an area-dependent resistance at the lipid head groups, rather than to a reduced partitioning at smaller area per lipid.[6,84] In addition, Mathai et al. found that the water permeability of DOPC/cholesterol membranes correlates with the area per lipid and suggested that both area-dependent resistance at the lipid head groups and alterations in the partition coefficient may contribute to this effect.[6]

To assess if the area per phospholipid, A_L, can explain the increase in $\Delta G_{w \to tails}$, we computed A_L for all membrane patches. Several methods have been proposed for how to distribute the total membrane area between phospholipids and cholesterol. Here, we computed the cholesterol area on the basis of the average tilt angle of cholesterol and assuming a cross section area of 0.38 nm² for cholesterol molecules, following the method of Alwarawrah et al.[85] The results are shown in Figure 5A demonstrating the decrease in A_L with [Chol] for all membranes, referred to as the condensing effect of cholesterol,[15] and in agreement with previous simulation studies.[22−24] For all lipids, the decreasing A_L indeed correlates with the increasing $\Delta G_{w \to tails}$ (Figure 4B−D), as reflected in a remarkable average (Pearson) correlation coefficient of $r = -0.88$ between A_L and $\Delta G_{w \to tails}$ (Figure 5B). In particular, the rapid decrease of A_L in DPPC upon the addition of 20−30% cholesterol (Figure 5A, blue) is in accord with the rapid increase in $\Delta G_{w \to tails}$ (Figure 4D). However, when comparing A_L of different phospholipid, not all features of $\Delta G_{w \to tails}$ can be explained by A_L. For instance, the decrease of A_L with [Chol] is similar in DMPC and POPC (Figure 5A, blue/green), yet $\Delta G_{w \to tails}$ increases more strongly in DMPC as compared to POPC (Figure 4B/C). In addition, note that A_L of pure POPE equals approximately A_L of POPC and DMPC with 30% [Chol], yet the barriers for all solutes are smaller in pure POPE than in these PC/cholesterol membranes. Finally, we note that we also derived A_L following the method of Hofsäß et al. and thus assuming a constant volume for cholesterol.[23] These
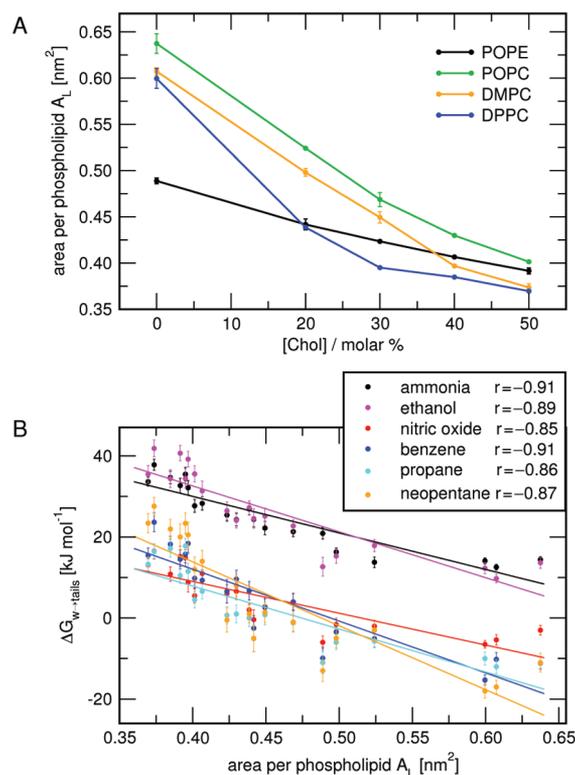

Figure 5. (A) Surface area per phospholipid A_L versus cholesterol content [Chol] in membranes of POPE (black), POPC (green), DMPC (yellow), and DPPC (blue). The decrease of the A_L visualizes the condensing effect of cholesterol. (B) Transfer free energy $\Delta G_{w \to tails}$ versus A_L. For each solute, a linear fit to the data points is plotted in the same color. Substantial correlation between $\Delta G_{w \to tails}$ and A_L is found, as indicated in the legend. The average correlation coefficient equals $r = -0.88$.

calculations yield a relatively weak correlation coefficient of -0.66 between A_L and $\Delta G_{w \to tails}$, suggesting that A_L based on the cholesterol tilt angle[85] provides a more accurate determinant for partitioning. On the basis of that analysis, we conclude that A_L is an important and intuitive determinant for partitioning into the lipid tail region, but that A_L alone does not quantitatively determine all the partition coefficients derived here.

An alternative determinant for permeability is the free volume inside the membrane,[7,24] because it would allow solute jumps between voids and hence facilitate solute diffusion.[86] For a quantitative analysis, however, the free volume is problematic because it depends on the size of the probe particle.[8] Theoretically, the free volume measured with a probe particle of the size of the considered solute would be related to the probability of finding that solute inside the membrane. Hence, that analysis would, first, simply yield an approximation to the PMF, without providing a structural interpretation of the PMF, and second, that analysis would converge extremely slowly because large voids are very rare in membranes with high cholesterol content.

Therefore, we here relate $\Delta G_{w \to tails}$ instead to the potential interaction energy V_{tails} between the lipid atoms in the lipid tail region (see Methods for details). V_{tails} quantifies the packing between lipid atoms, and V_{tails} must partly be overcome to insert a solute between lipid tails and/or cholesterol. Figure 6A shows V_{tails} per (heavy) lipid atom versus [Chol] for the 20 simulated membranes. V_{tails} per atom becomes stronger (more
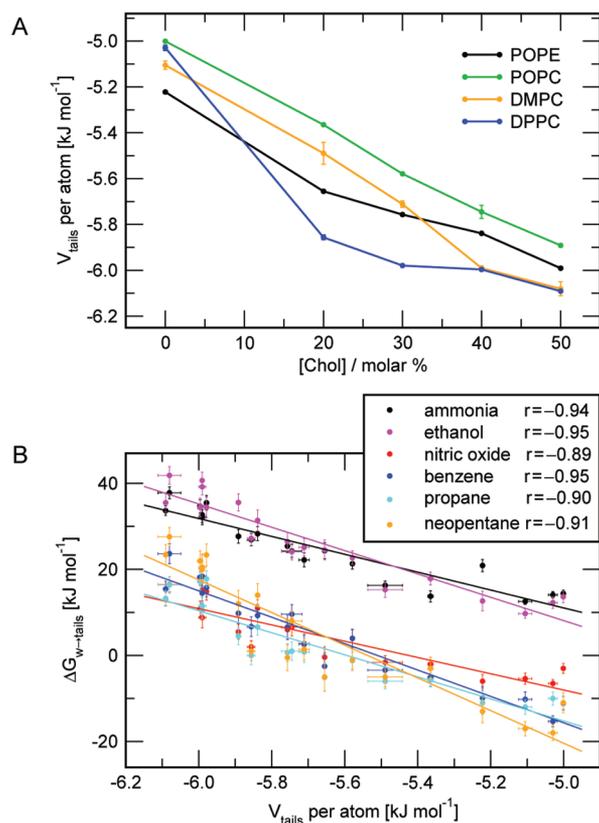
Figure 6. Lipid tail interaction as a determinant for solute partitioning. (A) Interaction energy V_{tails} per heavy lipid atom in the tail region versus cholesterol content. V_{tails} was computed from the equilibrium simulations of the membranes (see Methods for details). V_{tails} becomes stronger (more negative) with increasing cholesterol content [Chol], in line with the condensing effect of cholesterol on lipid membranes. (B) Transfer free energy $\Delta G_{w \rightarrow tails}$ versus the interaction energy V_{tails} per lipid atom. For each solute, a linear fit to the data points is plotted in the same color. Strong correlation between $\Delta G_{w \rightarrow tails}$ and V_{tails} is found, as indicated in the legend. The average correlation coefficient equals $r = -0.93$.

negative) with increasing [Chol] in all membranes, demonstrating the tighter packing of the membrane with [Chol], in line with the condensing effect of cholesterol. Figure 6B plots $\Delta G_{w \rightarrow tails}$ versus V_{tails} per atom, demonstrating high correlation between these two quantities. For DPPC, the strong decrease of V_{tails} between 0% and 30% [Chol] (Figure 6A, blue) is in accord with the strong increase of $\Delta G_{w \rightarrow tails}$ (Figure 4D). Likewise, for DMPC, the strong decrease of V_{tails} between 30% and 50% (Figure 6A, yellow) explains the respective strong increase of $\Delta G_{w \rightarrow tails}$ (Figure 4C). Moreover, for POPE, the substantial effect of [Chol] on $\Delta G_{w \rightarrow tails}$ (Figure 4A) is in line with the considerable decrease of V_{tails} (Figure 6A, black). In Figure 6B, the color of the dots encodes the solute, and to guide the eye, a fitted line to the data is shown for each solute in the same color. An average correlation coefficient of $r = -0.93$ between $\Delta G_{w \rightarrow tails}$ and V_{tails} is found, suggesting that the potential interaction energy between lipid atoms is an important determinant for $\Delta G_{w \rightarrow tails}$ and, hence, for solute partitioning. In addition, note that the slopes of the fitted lines for larger solutes such as ethanol or neopentane are more negative that the slopes for smaller solutes such as nitric oxide or ammonia. Hence, the partitioning of large solutes is more

sensitive to an increased lipid packing, in line with the findings in Figure 4.

The effect of lipid packing is further visualized in Figure 7, which illustrates the solvation of neopentane into a membrane of either pure DMPC (Figure 7A) or DMPC plus 50% cholesterol (Figure 7B). In the pure DMPC membrane, the lipid tails are highly disordered and interact only weakly with each other (Figure 7A, top). Consequently, upon the insertion of neopentane, the lipid tail structure is hardly affected and only few lipid–lipid interaction are required to break (Figure 7A, bottom). In contrast, in the presence of 50% cholesterol, the lipid tails are more ordered and form favorable van der Waals interactions to nearby cholesterol and other lipid tails, corresponding to a more negative V_{tails} (Figure 7B, top). Upon the insertion of neopentane, large van der Waals contacts between lipids are required to break (Figure 7B, bottom). In addition, the previously ordered tail structure is distorted, and large voids are formed above and below the neopentane (blue arrows). Together with the correlation analysis between $\Delta G_{w \rightarrow tails}$ and V_{tails} (Figure 6B), these results suggest that the increased packing in the lipid tail regions of cholesterol-containing membranes rationalizes the strong increase of $\Delta G_{w \rightarrow tails}$ with cholesterol content.

■ DISCUSSION

We have presented an extensive molecular dynamics study on the partitioning of six different solutes in cholesterol-containing lipid membranes. Twenty different membranes were simulated, composed of four different phospholipids plus an increasing cholesterol content between 0 and 50 mol %. The technique of umbrella sampling was employed to compute 120 PMFs for the permeation of the six solutes across these 20 membranes. The study required 5.8 μs of simulation time for the equilibration runs, and more than 150 000 umbrella histograms were extracted from 8.4 μs of umbrella sampling simulations, each histogram being based on 1 ns of simulation.

The local partition coefficient $K(z)$, the main determinant for membrane permeability, is directly related to the PMFs $G(z)$ via

$$K(z) = \exp[-G(z)/k_B T] \tag{2}$$

The four simulated phospholipids (POPE, POPC, DMPC, and DPPC) differ in headgroup size, tail length, tail saturation, and phase behavior, whereas the solutes differ in hydrophobicity and size. The 120 PMFs thus allow one to detect the effect of these lipid and solute properties on the partitioning in cholesterol-containing membranes. We found that, in all membranes, the partitioning into the very center of the membrane is hardly affected by the cholesterol content [Chol], whereas the partitioning in the lipid tail region is drastically reduced, suggesting that solutes accumulate in the bilayer center in the presence of cholesterol. Solute partitioning in the lipid tail region decreases with [Chol], irrespective of solute and membrane, but the magnitude of the decrease can differ substantially. The partitioning is more sensitive to [Chol] (a) for larger solutes, (b) in membranes with saturated as compared to membranes with unsaturated lipid tails, and (c) for membranes with smaller lipid head groups such as the PE as compared to the PC headgroup. A notable exception is represented by the DPPC membranes that formed the liquid ordered phase at [Chol] = 30% in the simulations. Adding more cholesterol to the liquid ordered phase did not lead to a further decrease in partitioning.
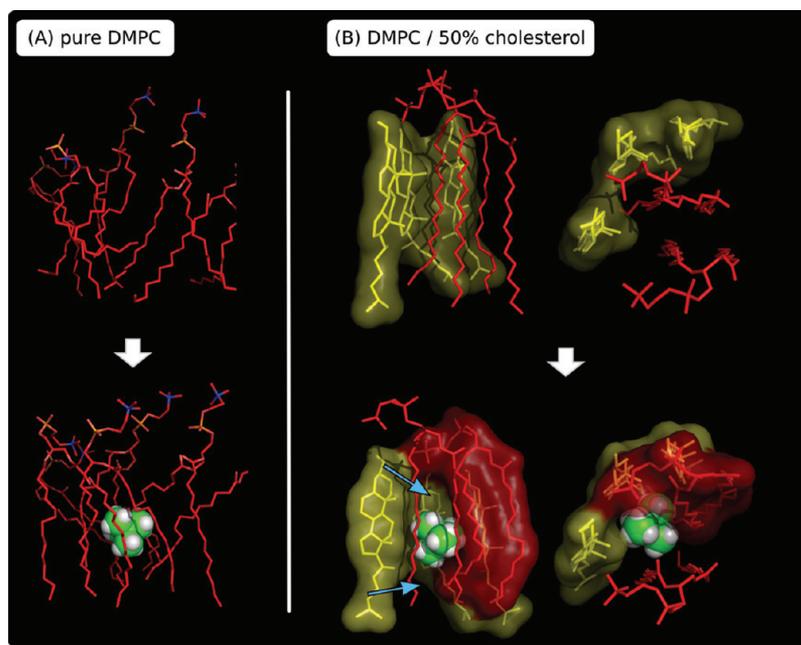
Figure 7. Solvation of neopentane into membranes of (A) pure DMPC and (B) DMPC plus 50% cholesterol. DMPC and cholesterol are shown as red and yellow sticks, respectively, and neopentane as green/white spheres. Some molecular surfaces are drawn in the same colors to visualize the molecular packing. In part B, the membrane is shown in side view (left) and top view (right). Lipid tails in pure DMPC are disordered (A, top) and the solvation of neopentane (A, bottom) does not alter the local membrane structure. With 50% cholesterol, the DMPC tails are highly ordered and form favorable van der Waals contacts to nearby cholesterol and other lipid tails (B, top). Here, the solvation of neopentane requires the rupture of large van der Waals contacts, the formation of voids above and below neopentane (blue arrows), and the distortion of the local membrane structure (B, bottom).

In addition, the large amount of data allows one to detect structural determinants for partitioning via correlation analysis. There is substantial correlation ($r = -0.88$) between the area per phospholipid A_L and the transfer free energy $\Delta G_{\text{w}\rightarrow\text{tails}}$ for moving a solute from water into the lipid tail region, in line with previous experimental studies.[32,35] However, when comparing membranes of different phospholipids, we found that A_L alone does not quantitatively determine the effect of [Chol] on $\Delta G_{\text{w}\rightarrow\text{tails}}$, suggesting that A_L only partially explains alterations in the partitioning. Instead, we found that the average potential energy between lipid tails and cholesterol explains much of the properties of $\Delta G_{\text{w}\rightarrow\text{tails}}$, as reflected in a high correlation coefficient ($r = -0.93$). Large favorable van der Waals contacts, as present in ordered membranes with high [Chol], must be broken for solute permeation and, thus, emerge as a quantitative determinant for membrane permeability.

A surprising finding of the present study is the magnitude of the effect of cholesterol on solute partitioning, which can be derived from eq 2, together with $\Delta G_{\text{w}\rightarrow\text{tails}}$ shown in Figure 4. Depending on the type of phospholipid and the size of the solute, the partition coefficient at the tails K_{tails} decreases by a factor of 10^2-10^7 upon the addition of 50% cholesterol (3×10^6 averaged over all solutes and membranes). The membrane permeability for hydrophilic solutes, which is limited by the partitioning into the hydrophobic lipid tail regions, is therefore also expected to decrease by several orders of magnitude. In contrast, experiments on macroscopic membranes typically derived a decrease in partitioning or permeability by only a factor of 2–6,[13,26−34,87] possibly by a factor of 25,[34,35] which is orders of magnitude weaker than the effect in the simulation. That discrepancy can hardly be explained by an uncertainty in the applied force field or simulation parameters. Likewise, our finding that the partitioning in the center of the bilayer is hardly affected by [Chol] cannot account for the difference to permeation experiments, because the permeability is limited by the highest barrier (or lowest partitioning) at the lipid tail regions, as follows from eq 1. Instead, we propose that a laterally inhomogeneous partition coefficient and permeability is required to explain the weak cholesterol effect in the experiments. In macroscopic membranes, the local cholesterol concentration [Chol] is not expected to be spatially and temporally constant but instead fluctuates due to lateral diffusion of cholesterol, complemented by temporary aggregation of (a few) cholesterol molecules and, under certain conditions, the formation of cholesterol lattice structures.[88,89] According to our PMFs, membrane areas with substantial local [Chol] display very low permeability and, hence, hardly contribute to solute flux across the membrane. However, membrane areas of low or zero local [Chol] would display a high local permeability similar to the respective pure phospholipid membrane.

As a simple quantitative model for the permeability of cholesterol-containing membranes we therefore suggest a two-area model. Accordingly, the total membrane area A is decomposed into an area $A_0(x)$ of zero local [Chol] and an area $A_{\text{chol}}(x)$ of substantial local cholesterol content, i.e., $A = A_0(x) + A_{\text{chol}}(x)$, where x denotes the average cholesterol mole fraction. Letting P_0 denote the permeability of the pure phospholipid membrane and approximating the permeability of A_{chol} by zero, the total permeability of the membrane is given by

$$P(x) = P_0 A_0(x)/A \qquad (3)$$

In that model, the experimental decrease of the permeability of macroscopic membranes with x reflects the decrease of $A_0(x)$, rather than the decrease of a laterally homogeneous membrane

permeability. Likewise, the more pronounced effect of cholesterol in membranes of saturated versus unsaturated lipids can be understood in terms of a more homogeneous distribution of cholesterol in saturated membranes, leading to a reduced $A_0(x)$ at equal x.

To validate our findings, experiments are required that detect the frequency of locally disordered membranes areas of low cholesterol content, rather than the ordering averaged over the entire membrane. Our results suggest that the occurrence of such disordered membrane patches correlates with the permeability of cholesterol-containing membranes. In addition, we suggest experiments on solute partitioning using spin-labeled lipids[13,32,33] but that differentiate between solutes in the vicinity of cholesterol and solutes surrounded by phospholipid tails only. Computationally, it will be highly interesting to compute the free energy and, hence, the probability for locally depleting cholesterol in a mixed cholesterol/phospholipid membrane. These approaches may yield a route to a detailed quantitative understanding of permeation across cholesterol-containing membranes.

■ ASSOCIATED CONTENT

ⓢ Supporting Information

Figures S1 and S2 demonstrate the convergence of $\Delta G_{\text{w}\rightarrow\text{tails}}$ versus equilibration time of the membrane patches and versus the equilibration of the umbrella simulations, respectively. Figure S3 compares three PMFs from umbrella sampling to PMFs recomputed using Widom's test particle insertion method. Figures S4 and S5 show nonsymmetrized PMFs. This material is available free of charge via the Internet at http://pubs.acs.org.

■ AUTHOR INFORMATION

Corresponding Author
jhub@gwdg.de

Present Addresses
[†]Department of Theoretical Physics, Royal Institute of Technology, SE-106 91 Stockholm, Sweden
[‡]Institute for Microbiology and Genetics, Georg-August-Universität Göttingen, Justus-von-Liebig-Weg 11, 37077 Göttingen, Germany

Notes
The authors declare no competing financial interest.

■ ACKNOWLEDGMENTS

■ REFERENCES

(1) Diamond, J. M.; Katz, Y. J. Membr. Biol. 1974, 17 (2), 121−154.
(2) Finkelstein, A. J. Gen. Physiol. 1976, 68 (2), 127−135.
(3) Walter, A.; Gutknecht, J. J. Membr. Biol. 1986, 90 (3), 207−217.
(4) Lande, M. B.; Donovan, J. M.; Zeidel, M. L. J. Gen. Physiol. 1995, 106 (1), 67−84.
(5) Xiang, T. X.; Anderson, B. D. Biophys. J. 1998, 75 (6), 2658−2671.
(6) Mathai, J. C.; Tristram-Nagle, S.; Nagle, J. F.; Zeidel, M. L. J. Gen. Physiol. 2008, 131 (1), 69−76.
(7) Marrink, S.-J.; Berendsen, H. J. C. J. Phys. Chem. 1994, 98, 4155−4168.
(8) Marrink, S. J.; Berendsen, H. J. C. J. Phys. Chem. 1996, 100 (41), 16729−16738.
(9) Bemporad, D.; Luttmann, C.; Essex, J. W. Biophys. J. 2004, 87 (1), 1−13.
(10) Bemporad, D.; Essex, J. W. J. Phys. Chem. B 2004, 108, 4875−4884.
(11) Sugii, T.; Takagi, S.; Matsumoto, Y. J. Chem. Phys. 2005, 123 (18), 184714.
(12) Orsi, M.; Sanderson, W. E.; Essex, J. W. J. Phys. Chem. B 2009, 113 (35), 12019−12029.
(13) Subczynski, W. K.; Hyde, J. S.; Kusumi, A. Proc. Natl. Acad. Sci. U. S. A. 1989, 86 (12), 4474−4478.
(14) Sackmann, E. In Structure and Dynamics of Membranes; Liposwski, R., Sackmann, E., Eds.; Elsevier, Amsterdam, 1995.
(15) Róg, T.; Pasenkiewicz-Gierula, M.; Vattulainen, I.; Karttunen, M. Biochim. Biophys. Acta 2009, 1788 (1), 97−121.
(16) Yeagle, P. Biochim. Biophys. Acta, Rev. Biomembr. 1985, 822 (3−4), 267−287.
(17) Yeagle, P. Biochimie 1991, 73 (10), 1303−1310.
(18) McMullen, T.; McElhaney, R. Curr. Opin. Colloid Interface Sci. 1996, 1 (1), 83−90.
(19) Edholm, O.; Nyberg, A. Biophys. J. 1992, 63 (4), 1081−1089.
(20) Robinson, A.; Richards, W.; Thomas, P.; Hann, M. Biophys. J. 1995, 68 (1), 164−170.
(21) Smondyrev, A.; Berkowitz, M. Biophys. J. 1999, 77 (4), 2075−2089.
(22) Chiu, S. W.; Jakobsson, E.; Mashl, R. J.; Scott, H. L. Biophys. J. 2002, 83 (4), 1842−1853.
(23) Hofsäß, C.; Lindahl, E.; Edholm, O. Biophys. J. 2003, 84 (4), 2192−2206.
(24) Falck, E.; Patra, M.; Karttunen, M.; Hyvönen, M. T.; Vattulainen, I. J. Chem. Phys. 2004, 121 (24), 12676−12689.
(25) Pandit, S. A.; Chiu, S.-W.; Jakobsson, E.; Grama, A.; Scott, H. L. Langmuir 2008, 24 (13), 6858−6865.
(26) Finkelstein, A.; Cass, A. Nature 1967, 216, 717−718.
(27) Mcelhaney, R. N.; de Gier, J.; van Deenen, L. L. Biochim. Biophys. Acta 1970, 219 (1), 245−247.
(28) Papahadjopoulos, D.; Nir, S.; Ohki, S. Biochim. Biophys. Acta, Biomembr. 1972, 266 (3), 561−583.
(29) Korten, K.; Sommer, T. J.; Miller, K. W. Biochim. Biophys. Acta 1980, 599 (1), 271−279.
(30) Smith, R. A.; Porter, E. G.; Miller, K. W. Biochim. Biophys. Acta 1981, 645 (2), 327−338.
(31) Luxnat, M.; Galla, H. J. Biochim. Biophys. Acta 1986, 856 (2), 274−282.
(32) De Young, L. R.; Dill, K. A. Biochemistry 1988, 27 (14), 5281−5289.
(33) Subczynski, W.; Wisniewska, A.; Yin, J.; Hyde, J.; Kusumi, A. Biochemistry 1994, 33 (24), 7670−7681.
(34) Antunes-Madeira, M. C.; Madeira, V. M. Biochim. Biophys. Acta 1985, 820 (2), 165−172.
(35) Xiang, T. X.; Anderson, B. D. J. Membr. Biol. 1995, 148 (2), 157−167.
(36) Jedlovszky, P.; Mezei, M. J. Phys. Chem. B 2003, 107 (22), 5322−5332.
(37) Eriksson, E. S. E.; Eriksson, L. A. J. Chem. Theory Comput. 2011, 7, 560−574.
(38) Pike, L. J. J. Lipid Res. 2003, 44 (4), 655−667.
(39) Risselada, H. J.; Marrink, S. J. Proc. Natl. Acad. Sci. U. S. A. 2008, 105 (45), 17367−17372.
(40) Ipsen, J. H.; Karlström, G.; Mouritsen, O. G.; Wennerström, H.; Zuckermann, M. J. Biochim. Biophys. Acta 1987, 905 (1), 162−172.
(41) Vist, M. R.; Davis, J. H. Biochemistry 1990, 29 (2), 451−464.
(42) Marsh, D. Biochim. Biophys. Acta 2010, 1798 (3), 688−699.
(43) Hub, J. S.; Winkler, F. K.; Merrick, M.; de Groot, B. L. J. Am. Chem. Soc. 2010, 132, 13251−13263.
(44) Jorgensen, W. L.; Chandrasekhar, J.; Madura, J. D.; Impey, R. W.; Klein, M. L. J. Chem. Phys. 1983, 79, 926−935.
(45) Van der Spoel, D.; Lindahl, E.; Hess, B.; Groenhof, G.; Mark, A. E.; Berendsen, H. J. C. J. Comput. Chem. 2005, 26, 701−1719.

(46) Hess, B.; Kutzner, C.; van der Spoel, D.; Lindahl, E. *J. Chem. Theory Comput.* **2008**, *4*, 435−447.

(47) Berger, O.; Edholm, O.; Jähnig, F. *Biophys. J.* **1997**, *72*, 2002−2013.

(48) Tieleman, D.; Berendsen, H. *Biophys. J.* **1998**, *74* (6), 2786−2801.

(49) Ulmschneider, J. P.; Ulmschneider, M. B. *J. Chem. Theory Comput.* **2009**, *5*, 1803−1813.

(50) Höltje, M.; Förster, T.; Brandt, B.; Engels, T.; von Rybinski, W.; Höltje, H. D. *Biochim. Biophys. Acta* **2001**, *1511* (1), 156−167.

(51) Jorgensen, W. L.; Maxwell, D. S.; Tirado-Rives, J. *J. Am. Chem. Soc.* **1996**, *118*, 11225−11236.

(52) Kaminski, G. A.; Friesner, R. A.; Tirado-Rives, J.; Jorgensen, W. L. *J. Phys. Chem. B* **2001**, *105*, 6474−6487.

(53) Cohen, J.; Arkhipov, A.; Braun, R.; Schulten, K. *Biophys. J.* **2006**, *91* (5), 1844−1857.

(54) Becke, A. D. *Phys. Rev. A* **1988**, *38*, 3098−3100.

(55) Lee, C.; Yang, W.; Parr, R. G. *Phys. Rev. B* **1988**, *37*, 785−789.

(56) Becke, A. D. *J. Chem. Phys.* **1993**, *98*, 5648−5652.

(57) Kendall, R. A.; Dunning, T. H. Jr.; Harrison, R. J. *J. Chem. Phys.* **1992**, *96*, 6796−6806.

(58) Woon, D. E.; Dunning, T. H. Jr. *J. Chem. Phys.* **1993**, *99*, 1914−1929.

(59) Frisch, M. J.; Trucks, G. W.; Schlegel, H. B.; Scuseria, G. E.; Robb, M. A.; Cheeseman, J. R.; Montgomery Jr., J. A.; Vreven, T.; Kudin, K. N.; Burant, J. C.; Millam, J. M.; Iyengar, S. S.; Tomasi, J.; Barone, V.; Mennucci, B.; Cossi, M.; Scalmani, G.; Rega, N.; Petersson, G. A.; Nakatsuji, H.; Hada, M.; Ehara, M.; Toyota, K.; Fukuda, R.; Hasegawa, J.; Ishida, M.; Nakajima, T.; Honda, Y.; Kitao, O.; Nakai, H.; Klene, M.; Li, X.; Knox, J. E.; Hratchian, H. P.; Cross, J. B.; Adamo, C.; Jaramillo, J.; Gomperts, R.; Stratmann, R. E.; Yazyev, O.; Austin, A. J.; Cammi, R.; Pomelli, C.; Ochterski, J. W.; Ayala, P. Y.; Morokuma, K.; Voth, G. A.; Salvador, P.; Dannenberg, J. J.; Zakrzewski, V. G.; Dapprich, S.; Daniels, A. D.; Strain, M. C.; Farkas, O.; Malick, D. K.; Rabuck, A. D.; Raghavachari, K.; Foresman, J. B.; Ortiz, J. V.; Cui, Q.; Baboul, A. G.; Clifford, S.; Cioslowski, J.; Stefanov, B. B.; Liu, G.; Liashenko, A.; Piskorz, P.; Komaromi, I.; Martin, R. L.; Fox, D. J.; Keith, T.; Al-Laham, M. A.; Peng, C. Y.; Nanayakkara, A.; Challacombe, M.; Gill, P. M. W.; Johnson, B.; Chen, W.; Wong, M. W.; Gonzalez, C.; Pople, J. A. *Gaussian 03, Revision C.02*; Gaussian, Inc., Wallingford, CT, 2004.

(60) Singh, U. C.; Kollman, P. A. *J. Comput. Chem.* **1984**, *5*, 129−145.

(61) Besler, B. H.; Merz, K. M. Jr.; Kollman, P. A. *J. Comput. Chem.* **1990**, *11*, 431−439.

(62) Bussi, G.; Donadio, D.; Parrinello, M. *J. Chem. Phys.* **2007**, *126* (1), 014101.

(63) Berendsen, H. J. C.; Postma, J. P. M; DiNola, A.; Haak, J. R. *J. Chem. Phys.* **1984**, *81*, 3684−3690.

(64) Miyamoto, S.; Kollman, P. A. *J. Comput. Chem.* **1992**, *13*, 952−962.

(65) Hess, B. *J. Chem. Theory Comput.* **2008**, *4*, 116−122.

(66) Darden, T.; York, D.; Pedersen, L. *J. Chem. Phys.* **1993**, *98*, 10089−10092.

(67) Essmann, U.; Perera, L.; Berkowitz, M. L.; Darden, T.; Lee, H.; Pedersen, L. G. *J. Chem. Phys.* **1995**, *103*, 8577−8592.

(68) Hess, B. *J. Chem. Phys.* **2002**, *116*, 209−217.

(69) Parrinello, M.; Rahman, A. *J. Appl. Phys.* **1981**, *52*, 7182−7190.

(70) Kumar, S.; Bouzida, D.; Swendsen, R. H.; Kollman, P. A.; Rosenberg, J. M. *J. Comput. Chem.* **1992**, *13*, 1011−1021.

(71) Hub, J. S.; de Groot, B. L.; van der Spoel, D. *J. Chem. Theory Comput.* **2010**, *6*, 3713−3720.

(72) Abraham, M. H.; Buist, G. J.; Grellier, P. L.; McGill, R. A.; Doherty, R. M.; Kamlet, M. J.; Taft, R. W.; Maroldo, S. G. *J. Chromatogr.* **1987**, *409*, 15−27.

(73) Liu, X.; Miller, M. J.; Joshi, M. S.; Thomas, D. D.; Lancaster, J. R. *Proc. Natl. Acad. Sci. U. S. A.* **1998**, *95* (5), 2175−2179.

(74) Li, J.; Carr, P. W. *Anal. Chem.* **1993**, *65*, 1443−1450.

(75) Marenich, A. V.; Kelly, C. P.; Thompson, J. D.; Hawkins, G. D.; Chambers, C. C.; Giesen, D. J.; Winget, P.; Cramer, C. J.; Truhlar, D. G. *Minnesota Solvation Database, version 2009*; University of Minnesota, Minneapolis, 2009.

(76) Hub, J. S.; de Groot, B. L. *Proc. Natl. Acad. Sci. U. S. A.* **2008**, *105* (4), 1198−1203.

(77) Widom, B. *J. Chem. Phys.* **1963**, *39*, 2808.

(78) Overton, E. *Vierteljahresschr. Naturforsch. Ges. Zürich* **1895**, *40*, 159−201.

(79) Kucerka, N.; Tristram-Nagle, S.; Nagle, J. F. *J. Membr. Biol.* **2005**, *208* (3), 193−202.

(80) Klauda, J. B.; Venable, R. M.; Freites, J. A.; O'Connor, J. W.; Tobias, D. J.; Mondragon-Ramirez, C.; Vorobyov, I.; MacKerell, A. D. Jr; Pastor, R. W. *J. Phys. Chem. B* **2010**, *114* (23), 7830−7843.

(81) Rappolt, M.; Hickel, A.; Bringezu, F.; Lohner, K. *Biophys. J.* **2003**, *84* (5), 3111−3122.

(82) Mateo, C. R.; Acuna, A. U.; Brochon, J. C. *Biophys. J.* **1995**, *68* (3), 978−987.

(83) Marqusee, J. A.; Dill, K. A. *J. Chem. Phys.* **1986**, *85*, 434−444.

(84) Nagle, J. F.; Mathai, J. C.; Zeidel, M. L.; Tristram-Nagle, S. *J. Gen. Physiol.* **2008**, *131* (1), 77−85.

(85) Alwarawrah, M.; Dai, J.; Huang, J. *J. Phys. Chem. B* **2010**, *114* (22), 7516−7523.

(86) Almeida, P. F.; Vaz, W. L.; Thompson, T. E. *Biochemistry* **1992**, *31* (29), 6739−6747.

(87) Waldeck, A. R.; Nouri-Sorkhabi, M. H.; Sullivan, D. R.; Kuchel, P. W. *Biophys. Chem.* **1995**, *55* (3), 197−208.

(88) Parker, A.; Miles, K.; Cheng, K. H.; Huang, J. *Biophys. J.* **2004**, *86* (3), 1532−1544.

(89) Chong, P. L.-G.; Zhu, W.; Venegas, B. *Biochim. Biophys. Acta* **2009**, *1788* (1), 2−11.